

Article

A Robust Denoised Algorithm Based on Hessian–Sparse Deconvolution for Passive Underwater Acoustic Detection

Fan Yin ^{1,2}, Chao Li ^{1,2,*}, Haibin Wang ^{1,2}, Shihong Zhou ^{1,2}, Leixin Nie ^{1,2} , Yonglin Zhang ^{1,2} and Hao Yin ^{1,2}

¹ State Key Laboratory of Acoustics, Institute of Acoustics, Beijing 100190, China

² School of Electronic, Electrical and Communication Engineering, University of Chinese Academy of Sciences, Beijing 100049, China

* Correspondence: chao.li@mail.ioa.ac.cn

Abstract: Digital beamforming techniques find wide applications in the field of underwater acoustic array signal processing. However, their azimuthal resolution has long been constrained by the Rayleigh limit, consequently limiting their detection performance. In this paper, we propose a novel two-dimensional Hessian–sparse deconvolution algorithm based on image processing techniques. This method assumes a priori that the underwater acoustic bearing time record (BTR) images exhibit sparsity, and then it first constructs partial differential equations in the beamforming domain with sparsity-norm constraints for optimal noise reduction. Subsequently, a two-dimensional deconvolution operation is applied to narrow the main lobe, aiming to achieve additional temporal gains in two-dimensional processing. The simulation and real sea trial data processing results show that the main lobe width of the proposed method is about 1.3 degrees at 0 dB. It effectively reduces the main lobe width and enhances the detection resolution of BTRs in the post-processing part, especially in low-signal-to-noise-ratio (SNR) environments. Therefore, the proposed method provides nice opportunities to further improve the target-detecting ability of hydrophone arrays.

Keywords: sparsity; Hessian matrix; noise cancellation; post-processing; deconvolution



Citation: Yin, F.; Li, C.; Wang, H.; Zhou, S.; Nie, L.; Zhang, Y.; Yin, H. A Robust Denoised Algorithm Based on Hessian–Sparse Deconvolution for Passive Underwater Acoustic Detection. *J. Mar. Sci. Eng.* **2023**, *11*, 2028. <https://doi.org/10.3390/jmse11102028>

Academic Editor: Rafael Morales

Received: 28 July 2023

Revised: 24 September 2023

Accepted: 20 October 2023

Published: 22 October 2023



Copyright: © 2023 by the authors. Licensee MDPI, Basel, Switzerland. This article is an open access article distributed under the terms and conditions of the Creative Commons Attribution (CC BY) license (<https://creativecommons.org/licenses/by/4.0/>).

1. Introduction

Underwater acoustic array signal processing techniques encompass beamforming, direction-of-arrival (DOA) estimations, and array parameter estimations. DOA techniques are particularly crucial in passive underwater acoustic detection as they serve as pre-processing for target detections, localization, recognitions, etc. Traditional DOA techniques rely on classical beamforming methods such as conventional beamforming (CBF) and minimum variance distortionless response (MVDR), which offer robust performance but suffer from the problem of low resolution caused by complex ocean environment noise. Furthermore, the various biological noises, ship noises, and other hydrodynamic noises in the ocean lead to low signal-to-noise ratios (SNRs), making it difficult to detect and track underwater targets. Within the real-world applications, it is hard to increase the array aperture to meet the needs of resolutions, and the ambient noise would never be controlled by users. Therefore, in this paper, we introduce image processing techniques and attempt to propose an effective and robust post-detection noise reduction method for underwater sound detection to facilitate underwater target-detecting tasks. This method can serve as a pre-enhancement technique for various high-resolution detection algorithms.

The deconvolution algorithm is a new DOA enhancing method that was first applied in underwater acoustic detection by TC. Yang [1] in 2017. It possesses rigorous theory and can effectively suppress the background noise and improve the resolution performance of CBF. The inventor [2] further combined it with principal component analysis (PCA) in order to adapt to lower-SNR environments. Based on these achievements, Xionghou Liu et al. [3] applied the deconvolution technique to two-dimensional forward-looking underwater acoustic imaging, further improving the resolution of both the angular dimension and

range dimension. Later, they [4] further applied it to multi-input multi-output underwater acoustic detection to achieve the same effect of suppressing side lobes, and provided a simple search method to optimize the point spread function (PSF) corresponding to the minimum range side lobe level after deconvolutions. Jie Huang et al. [5] proposed a new fast deconvolution beamforming algorithm that provides the possibility of real-time high-resolution beamforming for a multi-beam underwater acoustic detection system. Jeremy Dillon [6] proposed a theoretical model of the PSF for a multi-channel synthetic aperture detection array considering shadow cell beams and used this model to further perform deconvolution operations to remove grating lobe artifacts. Dajun Sun et al. [7] solved the problem that the existing Richardson–Lucy (R-L) method is only limited to the array with beam pattern translation invariance and proposed an extended R-L deconvolution algorithm that makes deconvolution CBF applicable to arrays with beam pattern direction changes, such as vector sensor linear arrays. Fei Wang et al. [8] proposed a combination of block sparsity and a complex-valued Bayesian compressive sensing method to improve the solving performance of complex-valued deconvolution beamforming. Simulation results showed that the proposed method produced a better beamforming performance for coherent targets compared to intensity-based deconvolution methods. Chao Ma et al. [9] proposed a deconvolution algorithm applied in the field of active underwater acoustic detection based on spatiotemporal two-dimensional information, improving the resolution capability of DOA under active detection from both time and angle dimensions. Peng Wang et al. [10] demonstrated that the output of conventional 3D beamforming can be represented as the convolution of the 2D array beam pattern used and the backscatter function of the imaging target in the far field and near field. They then used a deconvolution algorithm to improve the spatial resolution and suppress side lobes in the output of conventional beamforming. However, current research focuses more on replacing different iterative algorithms and applying deconvolution in various underwater acoustic fields, and there still exist some issues that are not well solved, such as a poor convergence of deconvolution iterations with low SNRs and the bottleneck of the Rayleigh limit.

In the field of image restoration, to address the problem of mixed noise removal and edge preservation, Rudin, Osher, and Fatemi [11] pointed out that the total variation of an image contaminated by noise is always greater than that of a noise-free image, and subsequently proposed the total variation (TV) regularization model. Tony F. Chan et al. [12] proposed a blind deconvolution algorithm based on TV minimization, and designed an alternating minimization implicit iterative scheme to recover the image while identifying the PSF. The results showed that the iterative method has good robustness, fast convergence (especially for discontinuous blur), and can achieve good recovery of both the image and PSF under noisy conditions. Antonin Chambolle [13] proposed a TV minimization algorithm and proved its effectiveness, further applying the algorithm to two standard inverse problems in image processing, namely image denoising and amplification. Shuo Huang et al. [14] improved the TV method by using a diffusion rate adjuster based on the phase consistency, a median filter, and a fusion filter with phase-consistent boundaries, which effectively prevents over-smoothing of the image when the iteration time exceeds the optimal value. Konstantinos [15] studied a non-local form of a TV-based faithful image denoising model, where the regular term is replaced by fractional-order TV, and discussed the regularity and uniqueness of the solution when the fidelity parameter is high or low. Rob Heylen et al. [16] explored the performance of a TV denoising-based 3D image denoising method in improving the pore segmentation of selective laser melting additive manufacturing parts. Donghao Lv et al. [17] proposed a new upper bound function to improve the accuracy of traditional TV denoising methods. Then, the enhanced TV denoising was used to update the algorithm based on TV denoising to improve the denoising efficiency. Arman et al. [18] improved the traditional Kalman filter by proposing a Kalman filter signal denoising framework that simultaneously uses conventional linear time-invariant filtering and TV denoising, which significantly improves the denoising effect. Meiniel et al. [19] proposed a novel sparsity-based image denoising algorithm that combines TV spatial regu-

larization, low-frequency information enhancement, and sparse estimation aggregation, which can handle simple and complex types of noise (Gaussian, Poisson, and mixed noise) without any prior model, only requiring a set of parameter values. Rabah et al. [20] used TV denoising to filter electrocardiogram signals, removing sharp edges and calculating the Morlet continuous wavelet coefficient matrix, which effectively distinguishes patients with cardiac diseases from normal electrocardiogram patients. However, there is currently a lack of research on directly applying TV denoising techniques to the backend of underwater acoustic-based deconvolution methods for noise suppression in acoustic BTRs.

In this paper, we introduce an image processing technique [21] to the CBF-based deconvolution algorithm and propose a Hessian–sparse deconvolution post-processing algorithm that can directly process two-dimensional BTRs to obtain more dimensional gain. This algorithm achieves good main lobe shrinking effects by avoiding the drawback of traditional deconvolution algorithms that converge too quickly in low SNRs environments, enhancing the target SNR, improving the visual effect of BTR, and making the target easier to detect visually or by other means. In the experiment, the main lobe width of the proposed method is only about 40% that of the CBF method at 0 dB. Compared to other image processing methods mentioned in previous studies, this method's advantages and innovations are:

- (a) To address the insufficient gain information in one-dimensional processing, the algorithm extends from one-dimensional deconvolution to two-dimensional deconvolution. It constructs a two-dimensional PSF to obtain additional processing gain.
- (b) In response to low signal-to-noise ratio issues, the algorithm successfully introduces partial differential equation denoising methods into the post-processing of underwater acoustic BTR. It considers underwater signal processing from an image processing perspective, thereby enhancing target detection gain.
- (c) To overcome the resolution bottleneck caused by the Rayleigh limit, the algorithm introduces a sparsity constraint term to model the underwater BTR process. This further reduces the width of the main lobe based on conventional deconvolution methods.

The remainder of this paper is organized as follows: Section 2 introduces two commonly used computational approaches for deconvolution algorithms. Section 3 introduces the principle of the proposed Hessian–sparse deconvolution method. Section 4 presents the simulation experimental results within different conditions. Section 5 processes real sea trial data to demonstrate the practicality of the algorithm in a marine environment. The final section summarizes the performance and innovation of the algorithm and highlights areas for potential improvements.

2. Related Works

In post-processing methods for DOA estimation in underwater acoustic detection, the introduction of deconvolution, as discussed in [1], has a significant impact. This approach utilizes principles of reconstruction from image processing and posits that the uncontaminated DOA should resemble a high-resolution pseudo-impulse signal. The conventional DOA spectrum is obtained after being affected by various underwater channel noises and interferences. Therefore, by employing the deconvolution concept in reverse modeling and using known array information to construct a prior PSF function, an effort is made to restore the originally narrow main lobe pseudo-impulse signal in one-dimensional DOA. Wei Bo et al. [22] introduced an accelerated deconvolution beamforming method for multi-beam synthetic aperture techniques. This method incorporates exponential acceleration and vector extrapolation to enhance the convergence speed of the classical R-L iteration. It accelerates the commonly used deconvolution R-L iterative algorithm, resulting in improved convergence. While these methods draw inspiration from concepts in image processing, they are still applied to one-dimensional DOA spectra. Consequently, this approach does not fully exploit the advantages of time accumulation gain and primarily contributes to spatial processing enhancements.

Fan et al. [23] employed an enhanced two-dimensional matched filter approach, drawing inspiration from matched filtering techniques commonly used in image processing. Initially, they curated a library of trajectory direction templates and subsequently applied post-processing directly to the two-dimensional BTR diagram, accumulated over the DOA. Moreover, in environments characterized by low SNRs, they implemented cascaded PCA denoising, retaining solely the first singular value from the singular value decomposition. This enabled the recovery of low-resolution trajectories, mitigating tracking vulnerabilities introduced by trajectory breakpoints. In the context of multi-target cross-interference underwater environments, the researchers [24] initially employed least-squares-based target motion analysis techniques to determine posterior directions for target trajectory motion. Subsequently, they enhanced the two-dimensional matched filter, initially based on linear interpolation, by introducing Gabor matched filtering. They leveraged the properties of the Gabor function, a Gaussian function modulated by a sine function, to design the template by solving parameters that ensured coherence between the beam response function and Gabor function. All of these methods harnessed both the temporal and spatial advantages of BTR. However, as the core of these methods still relies on traditional filters, further performance enhancements through various optimization algorithm theories have proven to be a challenging task.

3. Methods

In image processing applications, the deconvolution algorithm is widely used in various fields of image restoration, such as denoising and deblurring. Among them, the most commonly used methods for deconvolution are Wiener deconvolution based on frequency domain computation and RL iterative deconvolution based on spatial domain computation, which we will introduce in detail. Then, we present a systematic explanation of the proposed Hessian–sparse deconvolution technique based on image processing algorithms, specifically designed for underwater acoustic DOA estimation in this study. Subsequently, we provide a detailed introduction to the advanced iterative algorithm called split Bregman, which is a solution method for the proposed algorithm in underwater acoustic detection. The following diagram, Figure 1, illustrates the workflow framework of the entire proposed method.

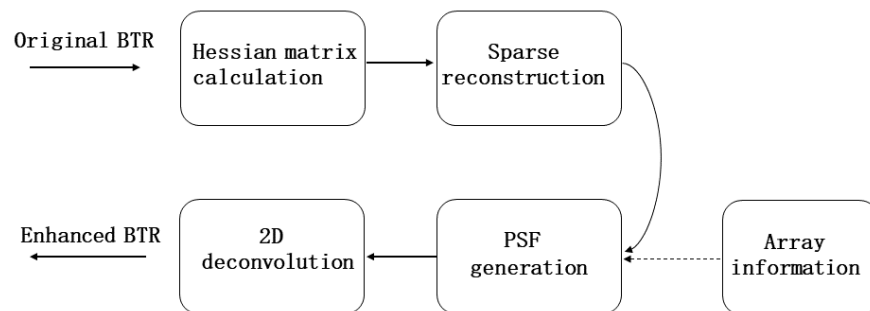


Figure 1. Block diagram of proposed method.

3.1. Wiener Deconvolution

The deconvolution algorithm is an image restoration method commonly used in image processing that maps the response function of the entire imaging system to a PSF, reducing the entire imaging process to the convolution of a real clean image and a PSF to produce the final system-generated image, expressed by the following equation:

$$g(x, y) = h(x, y) * f(x, y) \tag{1}$$

where $*$ is the convolution symbol, $g(x, y)$ is the degraded image, $f(x, y)$ is the real original image, and the channel response function $h(x, y)$ is the PSF and is expressed in the frequency domain as:

$$G(u, v) = H(u, v) \cdot F(u, v) \tag{2}$$

where $G(u, v)$, $H(u, v)$, $F(u, v)$ is the frequency domain expression of $g(x, y)$, $h(x, y)$, and $f(x, y)$, respectively. From the frequency domain representation, it is easy to obtain

$$F(u, v) = \frac{G(u, v)}{H(u, v)} \tag{3}$$

This is the process of deconvolution in the frequency domain, also known as Wiener deconvolution. However, as $H(u, v)$ is in the denominator, it must not take on a value of zero, and this results in a loss of part of the signal response. Therefore, when the PSF is known, it is used to adopt the RL iterative algorithm in the spatial domain instead. This space domain iterative deconvolution technique is flourishing in the field of image [25], radar [26], and other signal processing [27,28].

3.2. Deconvolved CBF and RL Iteration

The CBF algorithm is a robust and mature beamforming technique, widely used in passive underwater acoustic detection systems due to its high robustness to both array mismatch and data. Within the deconvolution theory, the CBF can be seen as the result of the convolution of the target source energy distribution and the array beam pattern.

$$B_{CBF}(\theta) = \int_{-\pi}^{-\pi} B_p(\theta|\vartheta)S(\vartheta)d\vartheta \tag{4}$$

where ϑ represents the direction of incidence of the target source under far-field conditions, θ is the direction of the beam response, $B_p(\theta|\vartheta)$ is the beam pattern function of the given array expressed in the form of a PSF, $S(\vartheta)$ is the full spatial energy distribution of the source signal, and $B_{CBF}(\theta)$ represents the DOA result, which is an estimate of the energy of the beam orientation.

The deconvolution process yields $B_{CBF}(\theta)$, which is the result of combining a known DOA with the array beam pattern $B_p(\theta|\vartheta)$. The array beam pattern can be computed by using array parameters. There are two main implementation algorithms for deconvolution: frequency domain and space domain. The Wiener deconvolution algorithm, as described in Section 1, is a frequency domain algorithm. On the other hand, space domain deconvolution is a technique mainly used in underwater acoustic detection. The RL iterative algorithm, which is based on Bayesian ideas, is an example of a space domain deconvolution technique and is commonly used in the field [29,30].

According to Equation (1), given the received BTR g and the PSF h of the receiving channel response, the original real BTR f can be estimated. According to Bayesian theory and the conditional probability formula, the estimated probability of f in the case that g has occurred is obtained as follows:

$$P(f_i|g_k) = \frac{P(g_k|f_i)P(f_i)}{P(g_k)} = \frac{P(g_k|f_i)P(f_i)}{\sum_j P(g_k|f_j)P(f_j)}; \quad i = \{1, I\}, j = \{1, J\}, k = \{1, K\} \tag{5}$$

where $j = \{1, J\}$ signifies that j is an integer variable with values ranging from 1 to J , inclusive. Here, J represents the total number of elements in its sample space. Similarly, I and K represent the total number of elements in their respective sample spaces. $P(f_i|g_k)$ is the probability of f_i being estimated under the condition that g_k occurs, $P(g_k|f_i)$ is the probability of g_k being estimated under the condition that f_i occurs, and $P(f_i)$ is the probability of f_i occurring.

$$P(f_i) = \sum_k P(f_i|g_k) = \sum_k P(f_i|g_k)P(g_k) \tag{6}$$

where $P(f_i g_k)$ is the joint probability of f_i and g_k , and $P(g_k)$ is the probability of g_k occurring. Because $P(f_i|g_k) = P(f_i g_k)/P(g_k)$, substitute Equation (5) into Equation (6), and then obtain

$$P(f_i) = \sum_k \frac{P(g_k|f_i)P(f_i)P(g_k)}{\sum_j P(g_k|f_j)P(f_j)} \tag{7}$$

In the equation above, both the left and right sides contain the term $P(f_i)$, which is the objective function that needs to be estimated. In practical applications of Bayesian theory, if $P(f_i)$ is unknown, an initial estimate of its value can be made using a priori knowledge. The above equation can then be written in iterative form:

$$P_{r+1}(f_i) = P_r(f_i) \sum_k \frac{P(g_k|f_i)P(g_k)}{\sum_j P(g_k|f_j)P_r(f_j)}, \quad r = \{0, 1, \dots\} \tag{8}$$

where r is the number of iterations. To use the above equation in iterative form, we need to estimate the initial value of $P(f_i)$. In Bayesian theory, if there is no prior knowledge available, it is common to assign a value similar to a more common probability distribution, such as the uniform distribution. The true estimate will then gradually converge to the true value through iterative steps.

Since $P(f_i) = f_i/f$ and $f = g$ (the sample space before and after image processing is of the same size), we have $P(g_k) = g_k/g = g_k/f$. Furthermore, $P(g_k|f_i) = P(h_{i,k}) = h_{i,k}/h$ and $h = \sum_j h_j, j = 1, J$; therefore, Equation (8) becomes

$$f_{i,r+1}/f = (f_r/f) \sum_k \frac{(h_{i,k}/h)(g_k/f)}{\sum_j (h_{j,k}/h)(f_{j,r}/f)} \tag{9}$$

The above equation can be simplified as

$$f_{i,r+1} = f_r \sum_k \frac{h_{i,k} g_k}{\sum_j h_{j,k} f_{j,r}} \tag{10}$$

The above array form is given as

$$f^{n+1}(x, y) = f^n(x, y) \left[\left(\frac{g(x, y)}{h(x, y) * f^n(x, y)} \right) * h(x, y) \right] \tag{11}$$

3.3. Hessian–Sparse Deconvolution

In this paper, we propose a Hessian–sparse deconvolution post-processing algorithm on top of a CBF-based deconvolution algorithm. This algorithm achieves excellent high-resolution BTRs even in low-SNR conditions. Although the inverse filtering model brings great convenience, it ignores additive noise, which has serious consequences. After analyzing the degradation function and noise statistics, we found that Wiener filtering works very well in image processing. However, it still exhibits sensitivity to noise. One of the prerequisites of image restoration based on Wiener filtering is that the image to be processed and the noise added to the image both follow the characteristics of a random process. Accurately deconvolving targets from BTR contaminated by ocean noise is often an ill-posed inverse problem. Therefore, we establish a constrained model using prior knowledge, hoping to make the deconvolution target trajectory as close as possible to their true positions.

In the field of image restoration, to solve the problem of mixed noise and edge preservation, Rudin, Osher, and Fatemi pointed out in 1990 that the total variation of a noisy image is always larger than that of a noise-free image. They further proposed the TV regularization model [11], which is shown below.

$$\arg \min_{x,b} \left\{ \frac{\lambda}{2} \|f - b - Ax\|_2^2 + \|\nabla_x\|_1 \right\} \tag{12}$$

where x can be seen as the BTR being reconstructed, f is the degraded BTR, A is the degradation operator, b is the estimation of the background noise in the BTR, and λ is a regularization parameter. The objective of this model is to find the BTR x that minimizes the total variation of x subject to the constraint that it fits the degraded BTR f according to the degradation operator A . The total variation is defined as the sum of the absolute differences in neighboring pixel values, which promotes image sparsity and edge preservation. The regularization parameter λ controls the trade-off between the data fidelity term (the first term) and the total variation term (the second term), where a larger value of λ results in a sparser image with more pronounced edges, but may also introduce more artifacts and noise.

In the experiment, the TV model achieved a good balance between noise removal and edge preservation. The enormous success and widespread application of TV algorithms over the past two decades can be attributed to their ability to preserve sharp edges. Furthermore, the convexity of the TV algorithm ensures that the algorithm has a stable solution. However, the piecewise constant solution of the TV algorithm model often causes a “staircase effect” in the denoising results, and the model does not consider the neighborhood information of pixels, using only the gradient magnitude as a measure of image smoothness. As a result, it cannot preserve the texture information of the image well. To eliminate the staircase effect, an increasing number of scholars are attempting to replace the TV algorithm with higher-order differential operator norms. The motivation behind this approach is to repair a larger range of images, not just the piecewise constant range. Many of these regularization terms include second-order differential operators, as the disappearance of piecewise second-order differentials allows the piecewise linear solution to better adapt to changes in smooth intensity, as shown in the Hessian matrix regularization in the above equation. The Hessian spectral norm not only protects the edges of the image well, but also restores the image to look smoother and more natural. This indicates that the Hessian spectral norm can achieve a good balance between edge preservation and suppression of the staircase effect.

$$\arg \min_{x,b} \left\{ \frac{\lambda}{2} \|f - b - Ax\|_2^2 + R_{Hessian}(x) \right\}, R_{Hessian}(x) = \left\| \begin{matrix} x_{tt} & x_{t\theta} \\ x_{\theta t} & x_{\theta\theta} \end{matrix} \right\| \quad (13)$$

where $R_{Hessian}(x)$ is a Hessian matrix that concerns the structural continuity of BTR x along the horizontal and vertical coordinates. t and θ , respectively, represent the temporal dimension variable and the azimuthal dimension variable of x . x_{tt} represents the second partial derivative of x with respect to the variable t , signifying the influence of changes in t on the curvature or convexity of x . $x_{\theta\theta}$ represents the second partial derivative of the BTR x with respect to the variable θ , indicating how changes in θ affect the curvature or convexity of x . $x_{\theta t}$ and $x_{t\theta}$ represent the cross-partial derivatives of θ and t , respectively. They are used to describe the mutual influence between t and θ .

The above equation is the objective function of a minimization problem with respect to x and the noise b . The goal is to find the values of x and b that minimize the function. The function is composed of two terms: a data fidelity term and a regularization term. The data fidelity term measures how well the linear operator A maps the variable x to the observed data f , which are corrupted by noise represented by the term b . The norm $\|f - b - Ax\|_2^2$ measures the difference between the observed data and the model prediction, and the factor $\frac{\lambda}{2}$ controls the trade-off between data fidelity and regularization. The regularization term $R_{Hessian}(x)$ is a penalty term that encourages certain properties of x . In this case, the regularization term involves the Hessian matrix of x , which is a matrix of second-order partial derivatives. The regularization term encourages x to have a smooth and natural appearance, and to preserve sharp edges while avoiding a staircase effect. The solution to this minimization problem can be found using various optimization techniques, such as gradient descent or conjugate gradient methods. The specific choice of optimization algorithm depends on the properties of the objective function and the computational resources available.

However, in deeper denoising processes, Hessian matrix regularization still inevitably affects resolution. In order to reduce background noise and further improve the resolution, we incorporate a sparse constraint term into the above equation based on the characteristic of target trajectory in underwater BTR satisfying the requirement of sparsity, resulting in the following form:

$$\arg \min_{x,b} \left\{ \frac{\lambda}{2} \|f - b - Ax\|_2^2 + R_{Hessian}(x) + \lambda_{L1} \|x\|_1 \right\} \tag{14}$$

where λ, λ_{L1} are scalar hyperparameters, f, b , and A are given data vectors and the matrix, $R_{Hessian}(x)$ is a regularization term that encourages a smooth solution, $\|\cdot\|_2$ denotes the L_2 norm (Euclidean distance), and $\|\cdot\|_1$ denotes the L_1 norm (sum of absolute values). To solve this problem, we can use the split Bregman algorithm [31], which has been widely used in TV problems due to its fast convergence speed. The block diagram of the proposed algorithm begins with inputting the original BTR as shown in Figure 1. Then, the algorithm calculates the Hessian matrix for the entire BTR image, obtaining second-order partial differentiation information for each pixel. Subsequently, it combines sparse regularization terms and employs Bregman iterations to optimize and reconstruct the denoised BTR. Then, it calculates the 2D PSF by using known array information, and conducts RL iterations on the reconstructed BTR to perform main lobe contraction. Finally, we obtain an enhanced BTR diagram with low background noise and a narrowed main lobe. From this, we obtain the overall flow of the Hessian–sparse deconvolution algorithm as shown in the Algorithm 1 below

Algorithm 1: Hessian–sparse deconvolution.

Input: Original BTR f

a. Use the split Bregman algorithm to calculate the following optimization formula:

$$\arg \min_{x,b} \left\{ \frac{\lambda}{2} \|f - b - Ax\|_2^2 + R_{Hessian}(x) + \lambda_{L1} \|x\|_1 \right\};$$

b. Calculate *PSF* from receive array information;

c. After obtaining the last x item, perform deconvolution iterative calculation and obtain the final x ;

return Reconstructed BTR x .

3.4. Split Bregman Algorithm

We utilize the split Bregman iteration algorithm to solve the aforementioned optimization problem in underwater acoustics. The algorithm is an iterative method mainly used for image restoration and denoising before. The split Bregman algorithm simplifies the post-processing of the underwater acoustic target detection by introducing auxiliary variables B and P , which separate the original problem into multiple independent subproblems. By combining L_2 norm regularization and data constraint terms, the algorithm preserves the smoothness of the image while retaining sparse gradient information, thereby achieving image restoration and denoising. It is based on the Bregman iteration concept and combines L_2 norm regularization and data constraint terms to effectively recover images with sparse gradients. The specific operation is as follows:

(a). The algorithm simplifies the solution process by decomposing the objective function into two subproblems. The objective function consists of a smoothness term related to the original image and an L_2 norm regularization term related to the image gradients. By introducing an auxiliary variable B and P , the objective function is split into two independent subproblems. (b). Iterative update of U (the BTR to be processed): in each iteration, U is updated by solving a quadratic regularization problem while keeping B and P fixed. This problem can be solved using methods like least squares, where the smoothness term is represented by the Euclidean norm and the data constraint term is represented by the L_2 norm. (c). Iterative update of B : in each iteration, B is updated by adding the gradient information to maintain consistency between U and P . (d). Iterative update of

P : in each iteration, P is updated by applying a soft thresholding function to modify the gradient information. The soft thresholding function sets values below a threshold to zero, thus preserving the sparse gradient information. (e). Termination criterion: the algorithm iterates until the change in U falls below a predefined threshold, indicating convergence.

The convergence and stability of the algorithm have been theoretically proven in relevant literature. Below is the pseudocode as shown in Algorithm 2 for the split Bregman algorithm used in the post-processing of underwater acoustic BTR:

Algorithm 2: Split Bregman iteration.

Input: Original BTR I , parameter λ , number of iterations $numIterations$

Initialization:

$U = I$ Split variable

$B = \nabla I$ Auxiliary variable for gradient information

$P = \nabla I$ Auxiliary variable for gradient information

$\epsilon = 1e - 6$ Convergence threshold

Iteration:

For $iter = 1$ to $numIterations$

Update U

$U_{prev} = U$

$U = \operatorname{argmin} U(\lambda \cdot \|P\|_1 + 0.5 \cdot \|U - I + B\|_2^2)$

Update B

$B = B + \nabla U$

Update P

$P = \operatorname{SoftThreshold}(\nabla U + B, \lambda)$

Check convergence

If $\|U - U_{prev}\|_2 < \epsilon$

break

EndIf

EndFor

Output: Return U

In the above pseudocode, ∇ denotes the gradient operator, $\|\cdot\|_1$ represents the L_1 norm, and $\|\cdot\|_2$ represents the L_2 norm. The *argmin* operator finds the value of U that minimizes the objective function, and *SoftThreshold* is a function that applies soft thresholding to its input. This pseudocode describes the basic flow of the split Bregman iteration algorithm.

4. Results and Discussion

In order to validate the algorithm's performance, we subsequently conducted validation using both simulated data and real sea trial data. In the simulation experiments, we conducted multiple sets of experiments under low SNRs and in multi-target cross-interference environments to explore the algorithm's performance boundaries. The results show that the proposed algorithm performs well in both scenarios.

4.1. Simulations

4.1.1. Low-SNR Environment

In this section, the algorithm's target enhancement ability under low-SNR conditions is evaluated. Frequency-dependent noise signals are used to generate ship radiation noise, and the SNR within the bandwidth is continuously modified. A speed of sound propagation of 1500 m/s is assumed, as well as $N = 32$ array elements spaced at $d = 0.75$ m, and a target rapidly moving in the range of 70 degrees to 110 degrees. The signal frequency band range is 100–1000 Hz, and the noise added during the experiments also falls within this frequency range. In the experiments, we calculated a one-dimensional PSF based on the corresponding array information. We then obtained a two-dimensional PSF by multiplying the transpose of the one-dimensional PSF by itself. In the simulation experiments, the horizontal axis of the BTR spans from 0 to 180 degrees with an angular resolution of 0.5 degrees. The vertical

axis represents a time duration of 400 s, with a time resolution of 1 s per frame of the DOA spectrum. In our experiments, we obtained a PSF matrix with a width of $L = 360$ based on the calculations, which aligns perfectly with the horizontal range of the BTR diagram. To meet the requirements of the deconvolution calculation, we need the length of the processed BTR to be greater than L . In this experiment, we chose a length of 400 s to fulfill the computational requirements. The sparse prior parameter for the proposed algorithm was set to 10, with 100 iterations for sparse reconstruction and 20 iterations for deconvolution RL, and we implemented the algorithm using MATLAB 2020a on a 64-bit Windows 11 operating system. The computer was equipped with a 12th Generation Intel(R) Core(TM) i7-12650H processor running at 2.30 GHz.

The MVDR beamformer significantly enhances performance in terms of multi-target resolution and interference suppression. However, the application of the MVDR beamformer in practical systems is not robust enough, especially when the number of snapshots is limited. It requires diagonal loading of the received signal covariance matrix, and different loading levels can lead to some loss in detection gain. Furthermore, the application of deconvolution theory in MVDR is not well developed. To ensure the robustness and theoretical interpretability of the practical system, we chose CBF as the baseline method. Then, the experiment compared the baseline methods: CBF and the one-dimensional deconvolution algorithm. We initially investigated the performance of the proposed algorithm and other methods in a high-SNR environment. The background SNR was set to 0 dB, and the SNR calculation used was the spectral SNR, which calculates the energy ratio between the signal and noise only within the corresponding frequency band. This approach provides a more accurate estimation of the SNR. Figure 2a shows the beamforming result at SNR = 0 dB in the element domain of the CBF. It can be seen that the formed beam has a wide main lobe. After a one-dimensional deconvolution operation as shown in Figure 2b, the main lobe width of the target trajectory is reduced, and the background noise is smoothed, but some noise artifacts are still visible. Figure 2c shows the result of the proposed method, which significantly reduces the main lobe width and the background noise. To obtain further quantitative results, the original image was sampled at a faster rate, as shown in Figure 2d. Because the highest frequency of the broadband signal is 1000 Hz, which is also the highest frequency commonly used in passive hydroacoustic detection, and the distance between the elements of the linear array is exactly half a wavelength, the 3 dB main lobe width of the CBF can be calculated to be approximately 6.0 degrees. The measured main lobe width of the deconvolution beam is 3.9 degrees, while the proposed method achieves a main lobe width of 1.3 degrees. It is clear that the processed results of the proposed method are significantly better than those of CBF and the one-dimensional deconvolution. Therefore, it can be concluded that under the current SNR condition, the proposed method can achieve a good main lobe reduction and background noise suppression effect.

To further explore the performance limits of the algorithm, we adjusted the background SNR down to -20 dB. Under such low SNR conditions, in order to highlight the algorithm's suppression of background noise, we took logarithms of all BTR images. As shown in Figure 3a, we can see that the background noise of the BTR is very high. Although the target trajectory can still be seen, the high noise obscuration will affect the accuracy of target detection and tracking. After one-dimensional deconvolution processing, the result is shown in Figure 3b. The background noise is reduced, but the boundary of the target trajectory is still not clear. The processing result of the proposed method is shown in Figure 3c. It can be seen that the background noise is greatly reduced, the energy of the target trajectory is significantly higher than that of the background noise, and the trajectory boundary is clear and visible. The results of a single snapshot experiment are shown in Figure 3d. The data show that the proposed method has reduced the background noise by about 10 dB compared to the original BTR, while the one-dimensional deconvolution processing has only reduced the background noise by about 3 dB. It can be seen that the proposed algorithm has a significant noise suppression effect. At the same time, under low-SNR conditions, the main lobe width of the proposed algorithm has a better shrinking

effect compared to CBF and one-dimensional deconvolution. Then, we conducted Monte Carlo repeated experiments under five different SNR environments, and calculated the numerical results for the 3 dB main lobe width. These results are listed in Table 1.

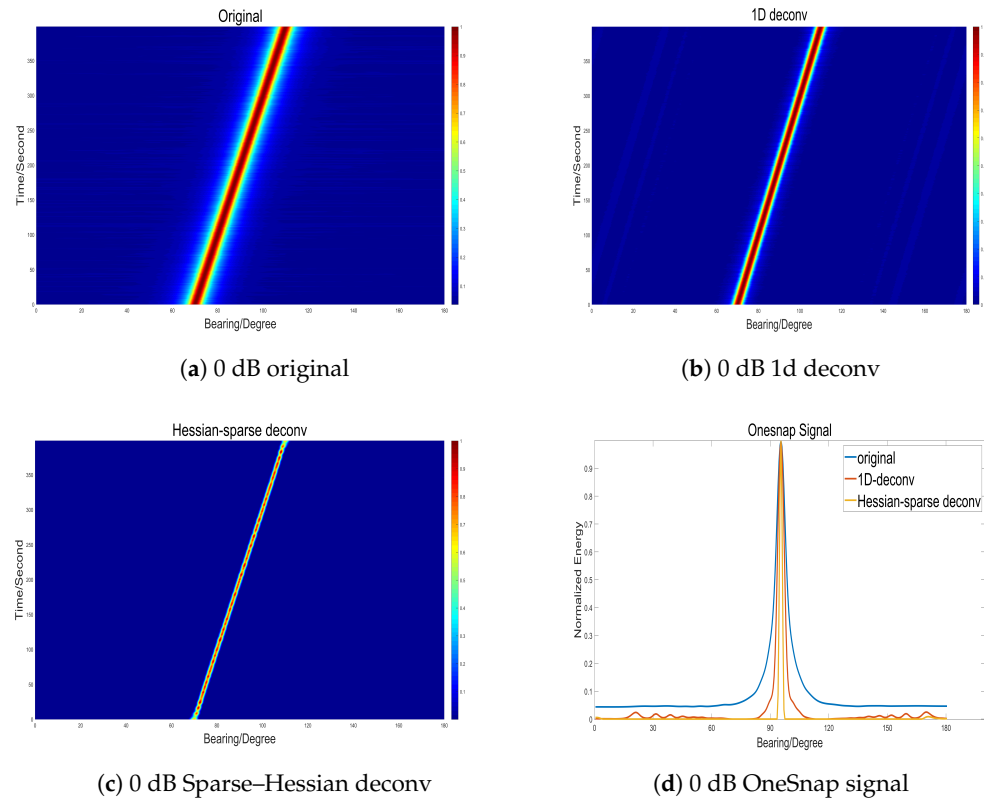


Figure 2. Experiment results under 0 dB.

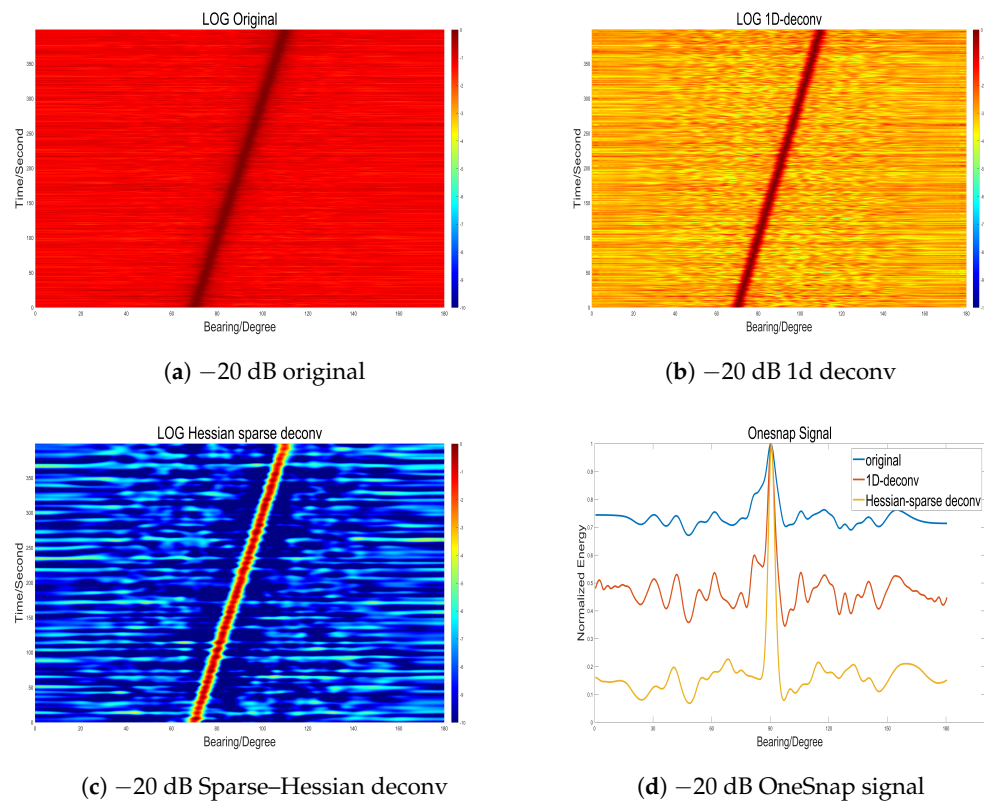


Figure 3. Experiment results under -20 dB.

Table 1. Beamwidth (degree) under different SNRs (wideband 100–1000 Hz).

SNR (dB)	CBF	Deconvolution	Proposed Method
0	6.0 degree	3.9 degree	1.3 degree
−5	6.3 degree	4.0 degree	1.8 degree
−10	8.9 degree	4.1 degree	2.0 degree
−15	11.3 degree	4.6 degree	3.1 degree
−20	14.8 degree	8.1 degree	4.1 degree

In the one-dimensional deconvolution experiment, the one-dimensional PSF is primarily used to shrink the beam in the spatial dimension, aiming to improve the resolution in visual representation. This indicates that one-dimensional deconvolution mainly focuses on spatial dimension processing by adjusting the beam shape to enhance the resolution of the BTR image. In contrast, in the two-dimensional deconvolution experiment, the two-dimensional PSF not only shrinks the beam in the spatial dimension but also contracts the target trajectory along the time axis. This feature is particularly helpful for scenarios involving fast-moving targets or motion blur. By incorporating time-axis processing, the two-dimensional deconvolution can effectively correct motion blur and enhance image clarity and resolution. Additionally, the application of two-dimensional deconvolution facilitates the integration of variational denoising and sparse optimization methods commonly used in image processing. These methods further reduce the influence of background noise and preserve more detailed information in the image, thereby improving the resolution. The combination of two-dimensional deconvolution with these denoising and optimization techniques leads to an enhanced performance in image processing.

4.1.2. Multi-Target Environment

In this section, the algorithm's ability to improve resolution is examined. Similarly, random noise signals are used to generate ship radiation noise, with a background signal-to-noise ratio of $SNR = 0$ dB. The number of elements is $N = 32$, the element spacing is $d = 0.75$ m, and 100–1000 Hz broadband beamforming is performed. There is a rapidly moving target at 90 degrees and another target rapidly moving in the range of 60 degrees to 120 degrees. The signal-to-interference ratio (SIR) between these two targets is 0 dB, indicating that their initial energy levels are comparable. This is reflected in the consistent main lobe width observed in the DOA spectrum. The comparison methods are CBF and a one-dimensional deconvolution algorithm.

The figure shown in Figure 4a presents the results of the CBF experiment. It can be observed that the background noise level is high in the processed data and the main lobe of the target trajectory is wide. At the edge of the intersection of the target trajectories (the 250th frame), it is difficult to distinguish according to the maximum energy principle. In Figure 4b, the one-dimensional deconvolution algorithm partially suppresses the background noise and further narrows the main lobe width, but it still cannot distinguish the trajectory intersection. Figure 4c shows the processing results of the proposed method, which significantly reduces the main lobe width of the target trajectory and suppresses the background noise noticeably compared to the other two methods. To further quantitatively analyze the experimental results, we extracted single-frame data at the edge of the target intersection and analyzed them, as shown in Figure 4d. It can be seen that the proposed method has the lowest background noise and narrowest main lobe width, and has a significant visual enhancement effect.

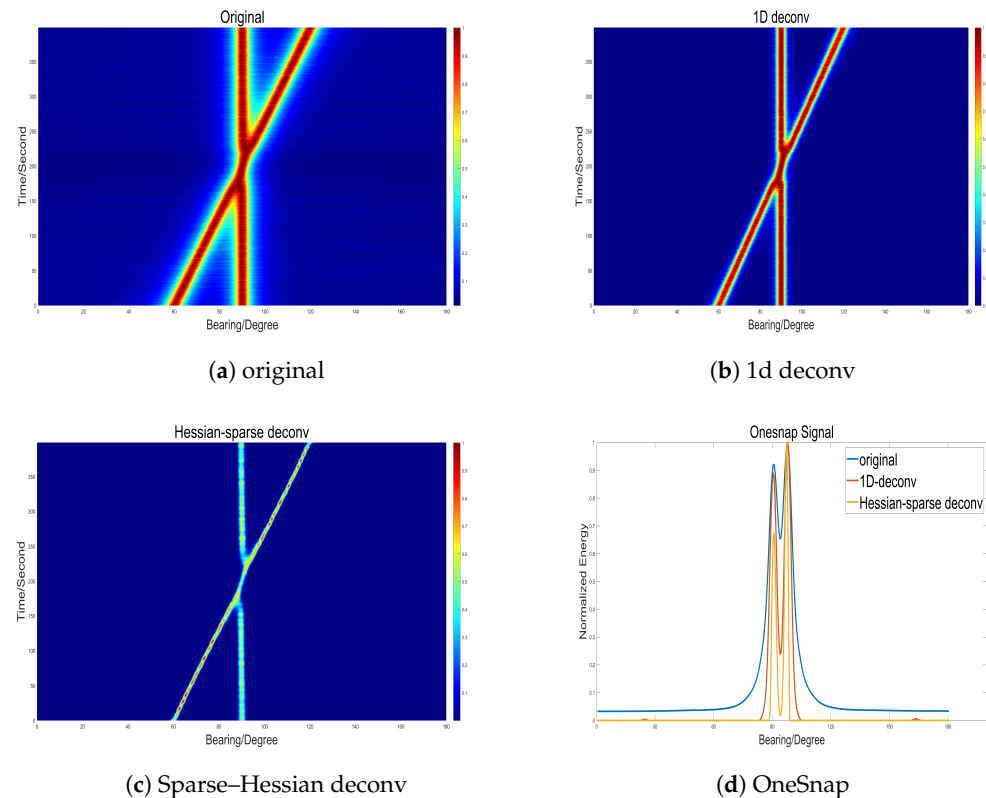


Figure 4. Experiment results under multi targets.

Based on the above analysis, it can be observed that this method still exhibits main lobe contraction effects in the presence of multiple interfering targets. The edge regions of the cross-interfering targets show relatively lower levels, resulting in a smoother removal of background noise. Visually, there is an overall improvement in the resolution of the targets. Further comparing the results for the two targets, although the initial main lobe widths are equal, the proposed method shows more pronounced main lobe contraction for the fast-moving target compared to the target at 90 degrees. The 2D deconvolution algorithm achieves contraction performance in the temporal dimension, effectively suppressing motion blur caused by fast-moving targets along the vertical scale. On the other hand, in the results obtained from the 1D deconvolution algorithm, there is no significant difference in the degree of contraction between the two target trajectories.

In simulation experiments, we first conducted algorithm performance verification under different SNRs. The proposed method demonstrated effective background noise suppression and main lobe contraction at an SNR of 0 dB, aligning with our experimental expectations. Further application of the proposed algorithm in an environment with an SNR of -20 dB revealed an outstanding performance in background noise suppression but a decline in main lobe contraction capability. Testing the proposed algorithm at an SNR of -26 dB showed unstable convergence, leading to potential distortion in target trajectories. The key distinction between this algorithm and traditional denoising methods is the simultaneous ability to contract the target’s main lobe while suppressing noise, providing additional benefits for subsequent operations. We quantified the main lobe contraction ability under various SNR environments, and the results, displayed in a table, indicate that the proposed method is less affected by noise compared to one-dimensional deconvolution algorithms. Additionally, the proposed method maintains a main lobe width below one-third of that achieved by CBF methods, relative to different environments. Next, to validate the algorithm performance in multi-target scenarios, we utilized simulated data with intersecting targets. The visual enhancement in target resolution was significant.

In multi-target environments, this resolution enhancement provides additional benefits for subsequent processing.

4.2. Sea Trials

In practical sea trial data, the complex marine environment (including various water surfaces, underwater vessels, marine organisms, etc.) results in significant background noise in the acquired BTRs; the background in sea trial data is much more complex compared to simulated experiments. This low-SNR environment not only affects the initial beamforming processing but also imposes serious limitations on the subsequent processing performance. In this section, we validate the reliability and stability of our proposed method using actual sea trial data obtained from experiments conducted in the South China Sea during the summer of 2021. The signal frequency band used in the experiment was 250–400 Hz, and a towed horizontal array consisting of 256 elements with an inter-element spacing of 1.5 m was employed for passive detection. We compared our proposed method with the CBF, deconvolution, and Hessian–sparse deconvolution methods, and further quantified and compared the BTR single-pulse processing results.

The three sets of experiments from left to right represent the results of beamforming using CBF, deconvolution, and Hessian–sparse deconvolution methods, respectively. It can be observed that the proposed Hessian–sparse deconvolution algorithm can significantly suppress background noise, shrink the main lobe width, and perform well in both noise suppression and resolution enhancement. To better compare the results, we extracted the single-frame data as shown in Figure 5d. It can be seen that the proposed method has a significantly narrowed beam and lower background noise energy. We zoomed in on the 30-degree position and showed it in the left frame. It can be seen that the CBF method cannot resolve the existence of weak targets, while both the deconvolution method and the proposed method can resolve them, and the proposed method has a clearer resolution. In addition, we can compare the 90-degree to 120-degree region and clearly see that the proposed method significantly outperforms the traditional CBF method in terms of background noise. This leads to a much clearer improvement in the visual effect of BTR.

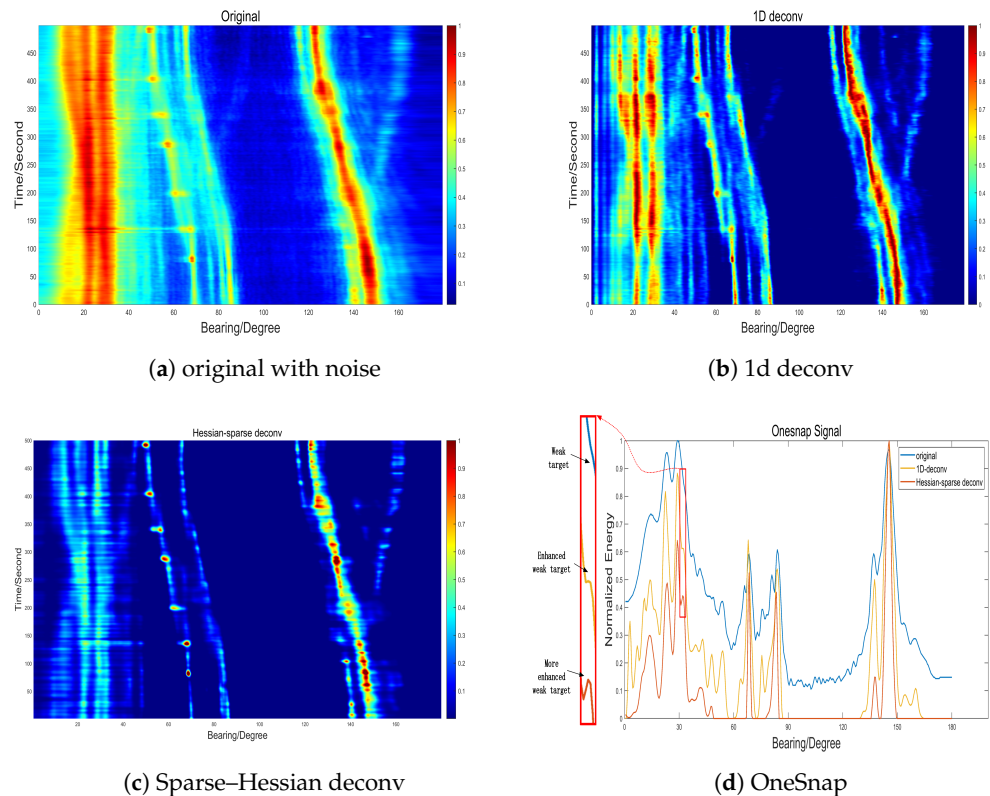


Figure 5. Experiment results under low SNR.

Besides the prominent target trajectories, there are some weak and scattered small targets between 140 degrees and 160 degrees, starting from 300 s. In the proposed algorithm, the introduction of a sparse regularization term causes some weak targets to be considered as affecting the overall sparsity during the iteration process and thus optimized out. This leads to the suppression of weak targets in that region. Therefore, there exists a trade-off between the introduction of sparsity and the preservation of weak targets. Further improvements may be required to make the proposed method suitable for applications involving the detection of extremely weak targets.

In sea trial data experiments, we observed that, compared to traditional CBF methods and one-dimensional deconvolution methods, the proposed method demonstrated a superior performance in background noise suppression and main lobe contraction for target trajectories. We also noted that, in single-shot data, weak targets that were challenging to detect using some traditional methods were distinguishable with the proposed method. In summary, one-dimensional deconvolution primarily improves spatial resolution by adjusting the beam shape, while two-dimensional deconvolution considers both spatial and temporal contraction, making it also suitable for addressing motion blur and similar issues. Both the simulation and sea trial experiments indicate that the proposed method significantly outperforms the other two methods. However, during the denoising and main lobe contraction processes, we observed some information loss or over-denoising. This instability is attributed to the settings of prior knowledge parameters and the choice of optimization iteration methods.

5. Conclusions

In the field of underwater detection, due to the complexity of ocean noise and the limitations of using array apertures, the obtained BTR often exhibits a low SNR and wide main lobes. In this paper, we propose a Hessian–sparse deconvolution method for denoising and beam pattern narrowing in underwater acoustic BTR diagrams. This method extends the one-dimensional deconvolution approach to two dimensions and incorporates noise reduction and resolution enhancement techniques from image processing by using optimization theory. More specifically, this method introduces Hessian matrices and sparse prior knowledge into the underwater BTR deconvolution process from an image processing perspective, providing a novel approach for resolution enhancement and noise suppression in the post-processing stage of underwater detection. However, due to the various factors in real-world scenarios that can lead to BTR degradation, the assumed prior information may not always be accurate. As a result, in practical sea trial data, we have observed that the proposed method, while effectively suppressing background noise and contracting the main lobe, may also suppress local information. In future research, we will further explore and investigate the construction of generic prior knowledge and strategies to avoid excessive denoising.

Author Contributions: F.Y.: Methodology, software, methodology, writing, investigation, writing—original draft preparation; C.L.: investigation, resources, data curation, project administration, and funding acquisition; H.W.: investigation, resources, writing—review and editing, supervision, project administration, and funding acquisition; S.Z.: investigation, writing—review and editing, supervision, and funding acquisition; L.N.: investigation, conceptualization, writing—review and editing; Y.Z.: investigation, conceptualization, writing—review and editing; H.Y.: investigation, writing—review and editing. All authors have read and agreed to the published version of the manuscript.

Funding: This research was supported by the National Key Research and Development Program of China (No. 2021YFC3101403), the National Natural Science Foundation of China (ID:62171440), and China Scholarship Council, Chinese Academy of Sciences.

Acknowledgments: The authors would like to thank the editors and reviewers for their comments on the manuscript of this article.

Conflicts of Interest: The authors declare no conflict of interest.

Abbreviations

The following abbreviations are used in this manuscript:

BTR	Bearing Time Record
DOA	Direction-of-arrival
CBF	Conventional Beamforming
MVDR	Minimum Variance Distortionless Response
PCA	Principal Component Analysis
SNR	Signal-to-Noise Ratio
PSF	Point Spread Function
R-L	Richardson–Lucy
TV	Total Variation

References

1. Yang, T.C. Deconvolved Conventional Beamforming for a Horizontal Line Array. *IEEE J. Ocean. Eng.* **2018**, *43*, 160–172. [[CrossRef](#)]
2. Yang, T.C. Deconvolution of decomposed conventional beamforming. *J. Acoust. Soc. Am.* **2020**, *148*, EL195–EL201. [[CrossRef](#)]
3. Liu, X.; Fan, J.; Sun, C.; Yang, Y.; Zhuo, J. High-resolution and low-sidelobe forward-look sonar imaging using deconvolution. *Appl. Acoust.* **2021**, *178*, 107986. [[CrossRef](#)]
4. Liu, X.; Shi, R.; Sun, C.; Yang, Y.; Zhuo, J. Using deconvolution to suppress range sidelobes for MIMO sonar imaging. *Appl. Acoust.* **2022**, *186*, 108491. [[CrossRef](#)]
5. Huang, J.; Zhou, T.; Du, W.; Shen, J.; Zhang, W. Smart Ocean: A New Fast Deconvolved Beamforming Algorithm for Multibeam Sonar. *Sensors* **2018**, *18*, 4013. [[CrossRef](#)]
6. Dillon, J. Grating lobe prediction and deconvolution for synthetic aperture sonar. *J. Acoust. Soc. Am.* **2018**, *144*, 1685. [[CrossRef](#)]
7. Sun, D.; Ma, C.; Yang, T.C.; Mei, J.; Shi, W. Improving the Performance of a Vector Sensor Line Array by Deconvolution. *IEEE J. Ocean. Eng.* **2020**, *45*, 1063–1077. [[CrossRef](#)]
8. Wang, F.; Tian, X.; Liu, X.; Gu, B.; Zhou, F.; Chen, Y. Combination Complex-Valued Bayesian Compressive Sensing Method for Sparsity Constrained Deconvolution Beamforming. *IEEE Trans. Instrum. Meas.* **2022**, *71*, 1–13. [[CrossRef](#)]
9. Ma, C.; Sun, D.; Mei, J.; Teng, T. Spatiotemporal two-dimensional deconvolution beam imaging technology. *Appl. Acoust.* **2021**, *183*, 108310. [[CrossRef](#)]
10. Wang, P.; Chi, C.; Liu, J.; Huang, H. Improving performance of three-dimensional imaging sonars through deconvolution. *Appl. Acoust.* **2021**, *175*, 107812. [[CrossRef](#)]
11. Rudin, L.I.; Osher, S.; Fatemi, E. Nonlinear total variation based noise removal algorithms. *Phys. D Nonlinear Phenom.* **1992**, *60*, 259–268. [[CrossRef](#)]
12. Chan, T.F.; Shen, J. *Image Processing and Analysis: Variational, PDE, Wavelet, and Stochastic Methods*; SIAM: Philadelphia, PA, USA, 2005.
13. Chambolle, A. An algorithm for total variation minimization and applications. *J. Math. Imaging Vis.* **2004**, *20*, 89–97.
14. Huang, S.; Wan, S. A Total Variation Denoising Method Based on Median Filter and Phase Consistency. *Sens. Imaging* **2020**, *21*, 19. [[CrossRef](#)]
15. Bessas, K. Fractional total variation denoising model with L1 fidelity. *Nonlinear Anal.* **2022**, *222*, 112926. [[CrossRef](#)]
16. Heylen, R.; Thanki, A.; Verhees, D.; Iuso, D.; Beenhouwer, J.D.; Sijbers, J.; Witvrouw, A.; Haitjema, H.; Bey-Temsamani, A. 3D total variation denoising in X-CT imaging applied to pore extraction in additively manufactured parts. *Meas. Sci. Technol.* **2022**, *33*, 045602. [[CrossRef](#)]
17. Lv, D.; Cao, W.; Hu, W.; Gan, C.; Wu, M. Denoising of piecewise constant signal based on total variation. *Neural Comput. Appl.* **2022**, *34*, 16341–16349. [[CrossRef](#)]
18. Roonizi, A.K.; Selesnick, I.W. A Kalman Filter Framework for Simultaneous LTI Filtering and Total Variation Denoising. *IEEE Trans. Signal Process.* **2022**, *70*, 4543–4554. [[CrossRef](#)]
19. Meinel, W.; Olivo-Marin, J.C.; Angelini, E.D. Denoising of microscopy images: A review of the state-of-the-art, and a new sparsity-based method. *IEEE Trans. Image Process.* **2018**, *27*, 3842–3856. [[CrossRef](#)]
20. Al Abdi, R.M.; Jarrah, M. Cardiac disease classification using total variation denoising and morlet continuous wavelet transformation of ECG signals. In Proceedings of the 2018 IEEE 14th International Colloquium on Signal Processing & Its Applications (CSPA), Penang, Malaysia, 9–10 March 2018; pp. 57–60.
21. Zhao, W.; Zhao, S.; Li, L.; Huang, X.; Xing, S.; Zhang, Y.; Qiu, G.; Han, Z.; Shang, Y.; Sun, D.E.; et al. Sparse deconvolution improves the resolution of live-cell super-resolution fluorescence microscopy. *Nat. Biotechnol.* **2022**, *40*, 606–617. [[CrossRef](#)] [[PubMed](#)]
22. Wei, B.; He, C.; Xing, S.; Zheng, Y. Accelerated Deconvolved Imaging Algorithm for 2D Multibeam Synthetic Aperture Sonar. *Sensors* **2022**, *22*, 6016. [[CrossRef](#)] [[PubMed](#)]
23. Yin, F.; Li, C.; Wang, H.; Yang, F. Automatic acoustic target detecting and tracking on the azimuth recording diagram with image processing methods. *Sensors* **2019**, *19*, 5391. [[CrossRef](#)] [[PubMed](#)]

24. Yin, F.; Li, C.; Wang, H.; Yang, F. Automatic Tracking of Weak Acoustic Targets within Jamming Environment by Using Image Processing Methods. *Appl. Sci.* **2022**, *12*, 6698. [[CrossRef](#)]
25. Sarder, P.; Nehorai, A. Deconvolution methods for 3-D fluorescence microscopy images. *IEEE Signal Process. Mag.* **2006**, *23*, 32–45. [[CrossRef](#)]
26. Zhao, S.; Shangguan, P.; Al-Qadi, I.L. Application of regularized deconvolution technique for predicting pavement thin layer thicknesses from ground penetrating radar data. *Ndt E Int.* **2015**, *73*, 1–7. [[CrossRef](#)]
27. Starck, J.L.; Pantin, E.; Murtagh, F. Deconvolution in astronomy: A review. *Publ. Astron. Soc. Pac.* **2002**, *114*, 1051. [[CrossRef](#)]
28. Levin, A.; Weiss, Y.; Durand, F.; Freeman, W.T. Understanding blind deconvolution algorithms. *IEEE Trans. Pattern Anal. Mach. Intell.* **2011**, *33*, 2354–2367. [[CrossRef](#)]
29. Richardson, W.H. Bayesian-Based Iterative Method of Image Restoration. *J. Opt. Soc. Am.* **1972**, *62*, 55–59. [[CrossRef](#)]
30. Lucy, L.B. An iterative technique for the rectification of observed distributions. *Astron. J.* **1974**, *79*, 745. [[CrossRef](#)]
31. Wang, Y.; Yang, J.; Yin, W.; Zhang, Y. A new alternating minimization algorithm for total variation image reconstruction. *SIAM J. Imaging Sci.* **2008**, *1*, 248–272. [[CrossRef](#)]

Disclaimer/Publisher’s Note: The statements, opinions and data contained in all publications are solely those of the individual author(s) and contributor(s) and not of MDPI and/or the editor(s). MDPI and/or the editor(s) disclaim responsibility for any injury to people or property resulting from any ideas, methods, instructions or products referred to in the content.